Geomechanics and Engineering, *Vol. 18, No. 1 (2019) 97-109*
DOI: https://doi.org/10.12989/gae.2019.18.1.097

Study on failure and subsidence law of frozen soil layer in coal mine influenced by physical conditions

Yaning Zhang*[1,2], Zhanbo Cheng[1,2,3a] and Huayong Lv[1,2a]

[1]School of Energy and Mining Engineering, China University of Mining and Technology (Beijing), Beijing 100083, China
[2]Coal Industry Engineering Research Center of Top-coal Caving Mining, Beijing 100083, China
[3]School of Engineering, University of Warwick, Coventry CV47AL, U.K.

(Received March 16, 2019, Revised April 29, 2019, Accepted April 30, 2019)

Abstract. Physical conditions play vital role on the mechanical properties of frozen soil, especially for the temperature and moisture content of frozen soil. Subsequently, they influence the subsidence and stress law of permafrost layer. Taking Jiangcang No. 1 Coal Mine as engineering background, combined with laboratory experiment, field measurements and empirical formula to obtain the mechanical parameters of frozen soil, the thick plate mechanical model of permafrost was established to evaluate the safety of permafrost roof. At the same time, FLAC^{3D} was used to study the influence of temperature and moisture content on the deformation and stress law of frozen soil layer. The results show that the failure tensile stress of frozen soil is larger than the maximum tensile stress of permafrost roof occurring in the process of mining. It indicates that the permafrost roof cannot collapse under the conditions of moisture content in the range from 20% to 27% as well as temperature in the range from -35°C to -15°C. Moreover, the maximum subsidence of the upper and lower boundary of the overlying permafrost layer decreases with the increase of moisture content in the range of 15% to 27% or the decrease of temperature in the range of -35°C to -15°C if the temperature or moisture content keeps consistent with -25°C or 20%, respectively.

Keywords: frozen soil; physical conditions; failure law; subsidence and stress laws

1. Introduction

In permafrost layer, the water exists as the form of ice due to the temperature below 0 °C. Therefore, the mechanical properties of frozen soil are significantly affected by the factors of temperature and moisture content, which are also greatly different from those of raw soil material with the existence of liquid water. At the same time, according to the formation time and existence period of frozen soil, it can be divided into three categories with short-term frozen soil, seasonal frozen soil and long-term frozen soil. It should be noted that permafrost areas account for approximately 25% of the Earth's land area where the rock strata are covered with thick frozen soil affecting the safety and stability of upper buildings and structures directly or indirectly as well as causing seriously interfere on underground construction and further triggering a variety of safety issues (Wang *et al.* 2017, Evans *et al.* 2018, Yao *et al.* 2019).

In recent decades, a large majority of scholars investigated the influence of temperature and moisture content on the mechanical properties of frozen soils presenting the strong correlation between them (Andersland and Akili 2015, Azadegan *et al.* 2014; Chen *et al.* 2016, Tu *et al.* 2016, Yoshimoto *et al.* 2016). To be specific, the compressive strength of frozen clay linearly and exponentially increased with the decrease of temperature and the increase of strain rate, respectively, through performing uniaxial compressive tests on saturated frozen clay with different dry densities at various strain rates and temperatures (Li *et al.* 2004). Moreover, the elastic modulus increased as well as the Poisson's ratio decreased, respectively, with the decrease of temperature (Dai *et al.* 2014). Christ and Kim (2009) carried out tensile tests to illustrate the effect of moisture content and temperature on the tensile strength of frozen silt with the temperature in the range from -20.0°C to -2.0°C, which represented the stress-strain behavior of frozen silt had strong dependence on the moisture content and temperature. Subsequently, Azmatch *et al.* (2011, 2012) carried out four-point bending tests to determine the tensile strength of the frozen fringe and its stress-strain behavior. The dependency degree of the tensile strength on temperature, deformation rate and unfrozen moisture content was also achieved. Meanwhile, Xu *et al.* (2018) proposed an extend constitutive model for frozen soil considering the temperature effect on the cohesion and strength properties of frozen soil on the basis of the hypoplastic constitutive model for sand. And the shear modulus of the frozen soil-rock mixture was nearly 3.7 times higher than that of the soil-rock mixture under normal temperature condition (Zhou *et al*. 2018).

On the other hand, a great deal of systematic theories had been established and proposed for predicting the law of surface subsidence and crack propagation (Hejmanowski and Malinowska 2009, Yang *et al*. 2016, Wang and Cheng 2016, Cheng *et al.* 2018, Liu *et al.* 2018, Sun *et al.* 2019,

*Corresponding author, Master Student
E-mail: yaningzhang@hotmail.com
[a]Ph.D. Student

http://www.techno-press.org/?journal=gae&subpage=7
ISSN: 2005-307X (Print), 2092-6219 (Online)

Liu and Cheng 2019, Lv *et al.* 2019). Ambrožič and Turk (2003) adopted the multi-layer feed-forward neural network for surface subsidence prediction, and the applicability of ANN had been verified in different subsidence models. Subsequently, Álvarez-Fernández *et al.* (2005) proposed a generalization of the n–k influence function within the context of mining subsidence simulation, which could carry out the shape of the expected subsidence trough better. Li *et al.* (2011) established a dynamic prediction model of surface movements based on the theory of support vector machines (SVM) and time series analysis to investigate the dynamic laws of surface movements due to mining activities in coal mines. Similarly, grey forecasting theory and grey prediction model was also adopted to forecast mining subsidence (Xu *et al.* 2014). Moreover, the arc tangent function model based on the "S" type settlement curves of the monitoring points in the collapsed pit and the failure mechanism of rock strata on the goaf was proposed (Nie *et al.* 2015). Xu *et al.* (2013) conducted mining-induced surface subsidence prediction by means of the finite difference method (FDM) to judge whether the extraction of the coal seam would have a negative impact on the dam. At the same period, Li *et al.* (2013) used probability integration and numerical simulation, which are the most commonly used methods in movement and deformation prediction, to compute ground subsidence deformation based on real measurement data.

However, it should be noted that the mechanical properties of frozen soil influenced by temperature and moisture content as well as mining subsidence are investigated as two separate systems in currently. Therefore, it is necessary to research the mining subsidence law of frozen soil layer as special engineering geology condition that its properties are influenced by temperature and moisture content. In this study, taking Jiangcang No. 1 Coal Mine as engineering background, laboratory experiments were carried out to obtain the basic mechanical parameters of frozen soil under different temperatures and water contents. Meanwhile, the thick plate mechanical model of permafrost layer was established and proposed to derive the failure criterion of frozen soil based on Vlazov thick plate theory. Lastly, numerical simulation was also performed to obtain the influence of temperature and moisture content on mining subsidence law of permafrost layer combined with the results of laboratory experiments and theoretical calculation.

2. Background

Jiangcang No. 1 Coal Mine is located in Gangcha County, Qinghai Province, China as shown in Fig. 1. Soil in mining area belongs to alpine frozen soil accompanied with high elevation and low temperature. To be specific, the altitude and minimum temperature are +3683 m and -34°C, respectively. Coal seam No. 20 is the main seam with an average thickness of 20 m and a dip angle of approximately 55° (Shang *et al.* 2017). The mining object as illustrated in Fig. 2 located in the middle of east and west open pit mines is coal pillar belonging to coal seam No. 20. And both of open pit mines have been already mined in the past several

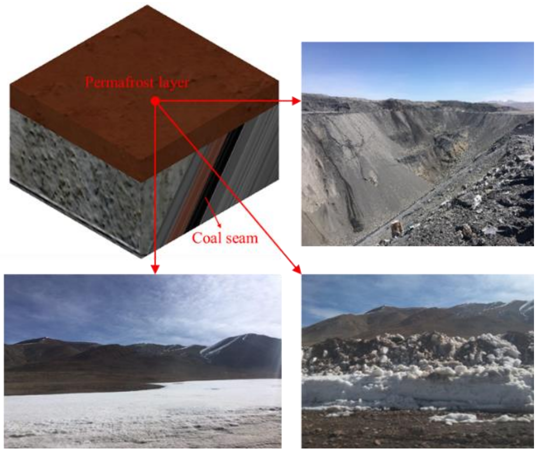

Fig. 1 Permafrost layer of Jiangcang No. 1 Coal Mine

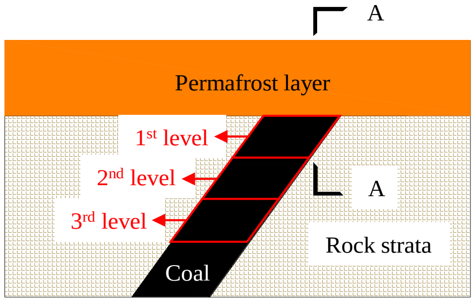

(a) Mining method

A-A section

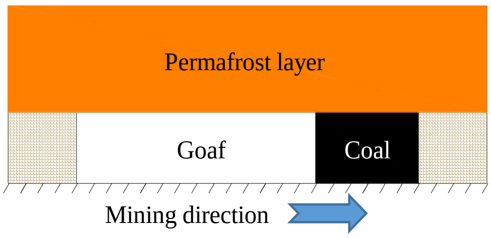

(b) Mining in first level

Fig. 2 Working face layout

years. Due to the large dip angle and thick coal seam of mining object, it is planned to use the steeply-inclined horizontal sublevel top-coal caving mining method to exploit coal seam. Therefore, it is divided into 3 levels with the height of each subsection 16 m, 17 m, 17 m, respectively, for downward mining. Moreover, the whole mining process is expected to be completed in a relatively short period within 4 months in winter because of the small reserves of this coal pillar.

In terms of overlying permafrost layer, it is relatively flat with an average thickness of 30m (Suo and Fan. 2014). However, there is a seasonal thawing layer in the range from 1.5 m to 1.7 m thick above permafrost layer. And it would be thawed under high temperature, especially during the summer months each year. However, the average melting rate is 0.01 m/d. Therefore, the influence of the seasonal thawing layer can be negligible because of the relatively thinner thickness compared with thick permafrost layer, especially in winter with low temperature.

Moreover, the mechanical properties of permafrost layer mainly depend on the factors of temperature and moisture content. However, its temperature is basically stable below -5 °C and -15°C in summer and winter, respectively. And the geothermal gradient of permafrost layer is 0.027°C/m ~ 0.042°C/m, as a result, just 0.81°C ~ 1.26°C changing can be found in 30m-thick permafrost layer. Therefore, it is reasonable to neglect the change of temperature in permafrost layer. At the same time, the moisture content of permafrost layer in Jiangcang No. 1 Coal Mine is over 20%. Thus, it is necessary to investigate the broken structure and subsidence laws of overlying permafrost layer for performing coal mining activities security and economic under these special geology conditions.

3. Basic mechanical parameters of frozen soil

The basic mechanical parameters of frozen soil include elastic modulus, Poisson's ratio, compressive strength, tensile strength, cohesion and internal friction angle. Especially, uniaxial compression testing can be carried out to obtain the unconfined compressive strength and derive the value of elastic modulus according to the behavior of stress-strain curve. Both of values are influenced by the factors of temperature and moisture content. However, except for both values, other parameters can be obtained from field measurements or empirical formula.

3.1 Experimental work

Remolded standard cubic frozen soil specimens with the size of 10 cm × 10 cm × 10 cm, which is similar to the properties of overlying permafrost layer in Jiangcang No. 1 Coal Mine, are performed to study the variation law of mechanical properties with temperature and moisture content (the quality ratio of water to soil). And the physical and mechanical properties of selected mild clay are shown in Table 1. Meanwhile, the particle size distribution of selected mild clay is shown in Fig. 3. Although cubic specimens show different failure patterns and levels of failure strength compared to cylindrical samples, they were chosen for this study because they are easier to test in numerous cases in terms of specimen preparation and test performance (Chang *et al.* 2015; Viso *et al.* 2008).

Moreover, uniaxial compressive tests were carried out with different temperature and moisture content to acquire the values of unconfined compressive strength and elastic modulus. It should be noted that the moisture content in this paper refers to the corresponding value of soil in unfrozen status. For investigating the influence of temperature on the mechanical properties of frozen soil, five categories temperatures of -15°C, -20°C, -25°C, -30°C, and -35°C were selected as research objects and the specimens were placed in corresponding temperature with 48 hours as well as the moisture content kept consistent with 20% in each sample. On the other hand, the values of moisture content with 15%, 20%, 22%, 25% and 27% were adopted and the temperature kept consistent with -25°C along with all specimens also placed in the specific condition for 48 hours to investigate the factor of moisture content how to affect the unconfined compressive strength and elastic modulus of

Table 1 Physical and mechanical properties of selected mild clay

Classification	Dry density (g/cm^3)	Void ratio	Elastic modulus (MPa)	D_{50} (μm)	C_c	C_u
mild clay	1.7	0.6	34 ~ 69	73.68	1.09	4.78

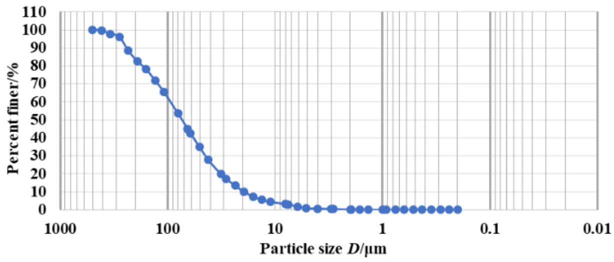

Fig. 3 The particle size distribution of mild clay

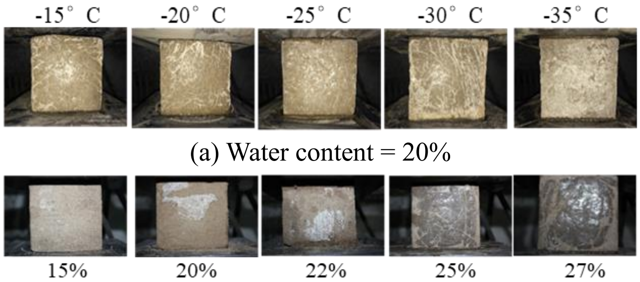

(a) Water content = 20%

(b) Temperature = -25°C

Fig. 4 Frozen soil specimens

Fig. 5 Experimental equipment

frozen soil specimens as shown in Fig. 4.

Five specimens were measured and calculated to obtain the average value in order to ensure the accuracy of result in same temperature and moisture content. The WAW-600B micro-computer controlled electro hydraulic servo universal testing machine was used in this study as shown in Fig. 5. It is mainly composed of the following parts: 600kN axial actuator, axial load and displacement transducers, screen display and testing results treatment. The device can be regarded as a rigid test machine because the failure strengths of the frozen soil are very small in relation to the measurement range of the test apparatus. Therefore, it meets the requirement of the International Society for Rock Mechanics (Hatheway 2009). During the experimental loading process, the strain rate used for all the specimens was 10 mm/min to make sure the loading time was around 2 minutes only. At the same time, heat insulated foam plates were wrapped around the upper and lower loading plates for ensuring the temperature of specimens remaining constant, too.

Table 2 Uniaxial compression test results with different temperatures and moisture contents

Temperature/°C	Moisture content/%	Number of specimens	Average uniaxial compressive strength /MPa	Average elastic modulus/MPa
-15			3.81	116.97
-20			5.10	119.01
-25	20	5	5.35	151.03
-30			6.52	193.46
-35			7.59	219.37
	15		3.22	122.20
	20		5.35	151.03
-25	22	5	6.37	169.10
	25		7.61	201.18
	27		8.53	221.72

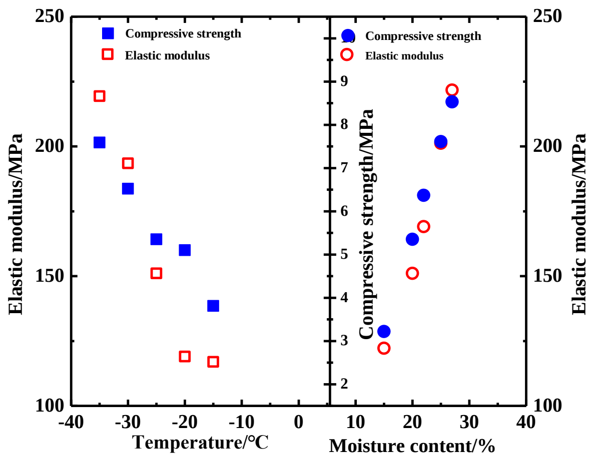

Fig. 6 Mechanical parameters versus temperature or moisture content

3.2 Unconfined compressive strength and elastic modulus

The results of unconfined compressive strength (UCS) and elastic modulus in uniaxial compression tests with different temperature and moisture content are described in Table 2. Based on the limited data, it can be found that both of uniaxial compressive strength and elastic modulus of frozen soil increase with the decrease of temperature. In opposite, the increase of moisture content causes both of values increasing.

The regression curves (Fig. 6) of uniaxial compressive strength and elastic modulus of frozen soil versus temperature with the conditions of moisture content keeping 20% can be expressed as follows. And the fitting type is consisting with Li *et al.* (2004).

$$R_c = 2.4525e^{-0.032T} \tag{1}$$

$$E = 64.788e^{-0.035T} \tag{2}$$

where R_c and E are uniaxial compressive strength and elastic modulus of frozen soil specimens, respectively. T is the temperature of frozen soil specimens.

Meanwhile, the relationship between the mechanical properties of frozen soil and temperature and its corresponding fitting curves with the conditions of temperature keeping -25°C are drawn in Fig. 6 as well. And the relative expressions can be shown in Eqs. (3) to (4).

$$R_c = 1.006e^{0.0811\omega} \tag{3}$$

$$E = 56.406e^{0.0504\omega} \tag{4}$$

where ω is moisture content of frozen soil specimens.

3.3 Other mechanical parameters

3.3.1 Bulk modulus and shear modulus

Bulk modulus (K) and shear modulus (G) are two crucial mechanical parameters in numerical simulation. However, they can be described by the variables of elastic modulus and Poisson's ratio as follows

$$K = \frac{E}{3(1-2\mu)} \tag{5}$$

$$G = \frac{E}{2(1+\mu)} \tag{6}$$

where E and μ are elastic modulus and Poisson's ratio of frozen soil, respectively. And μ can be regards as 0.35 for frozen soil.

3.3.2 Cohesion and internal friction angle

The shear properties of materials mainly depend on the instinct parameters of cohesion and internal friction angle which are varied with the temperature and moisture content as follows

$$c = \left(m_1 + |T|^{m_2}\right) \times \left(m_3 + \omega^{m_4}\right) \tag{7}$$

$$\varphi = A|T| + B \tag{8}$$

where T and ω are temperature and moisture content of frozen soil. m_1, m_2, m_3 and m_4 are fitting parameters. In this paper, m_1, m_2, m_3, m_4 are adopted to 214.3, 1.665, 0.167, 0.122, respectively. Meanwhile, A and B are regarded as 0.607 and 27.25, respectively. Therefore, by substituting the values of temperature and moisture content into Eqs. (7) and (8), the cohesion and internal friction angles under these conditions can be obtained.

3.3.3 Tensile strength

The tensile strength of soil or rock is generally smaller than other mechanical parameters. Therefore, it can be adopted as a criterion value for evaluating the failure of geotechnical materials in engineering practices. Eq. (9) is listed for obtaining the tensile strength of frozen soil.

$$R_t = \frac{R_c}{K} \tag{9}$$

where R_t and R_c are tensile strength and uniaxial compressive strength of frozen soil, respectively.

Table 3 Mechanical parameters of frozen soil with different temperatures and moisture contents

Temperature/°C	Moisture content/%	*K*/MPa	*G*/MPa	*c*/MPa	φ/°	R_t/MPa
-15	20	129.97	43.32	0.30	36.36	0.19
-20		132.23	44.07	0.36	39.39	0.25
-25		167.81	55.94	0.42	42.43	0.27
-30		214.96	71.65	0.50	45.46	0.33
-35		243.74	81.25	0.58	48.50	0.38
-25	15	135.78	45.26	0.41	42.43	0.16
	20	167.81	55.94	0.42	42.43	0.27
	22	187.89	62.63	0.43	42.43	0.32
	25	223.53	74.51	0.43	42.43	0.38
	27	246.36	82.12	0.44	42.43	0.43

K is the ratio of uniaxial compressive strength to tensile strength, and in this study, *K* is selected as 20.

According to the above analysis and described, combined with the experiment results of uniaxial compressive strength of frozen soil varying with temperature and moisture content, the other mechanical parameters, such as bulk modulus, shear modulus, cohesion, internal friction angle and tensile strength varying with temperatures and moisture contents are shown in Table 3.

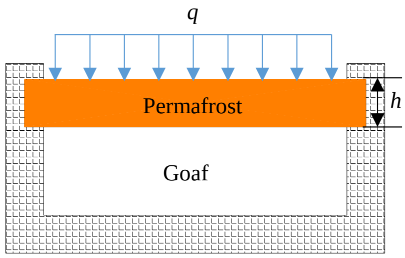

Fig. 7 Simplified thick plate mechanics model

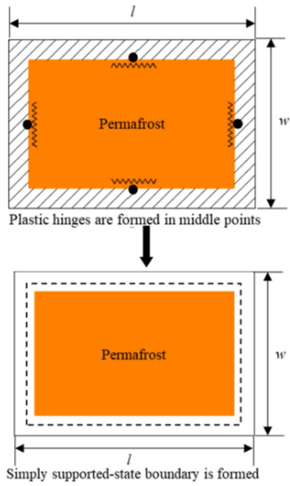

Fig. 8 Fixed-state boundary to simply supported-state boundary

4. Thick plate mechanical model of overlying permafrost

The overlying permafrost roof may collapse as a result of its own gravity causing serious mining accidents. In order to evaluate the safety of the permafrost roof, the thick plate mechanical model of overlying permafrost is established.

4.1 Theoretical model established

In general, the roof can be regards as elastic beam which has been applicable in the fields of rock burst and roof instability analysis (Qin *et al.* 1999). However, the reliability of the results cannot be guaranteed and the limitation is obvious because this calculation method is very simply as a result it is not enough to reflect the spatial effect and anisotropy of the roof. Therefore, it is more reasonable that elastic plate is adopted to describe the roof in stope. According to the ratio of roof thickness to span, the roof of stope can be regards as two categories of thin plate and thick plate. However, it is certainly limitation for thin plate due to lack in taking account of shear deformation at the end of the plate. Moreover, Cheng (1989) proposed that the mechanical theory of thick plate should be taken if the ratio of thickness to span is greater than 1/5 to 1/8. In this study, the Vlazov thick plate theory is used to evaluate the stability of permafrost roof. In general, the roof usually has two forms of failure with tensile and punching. Therefore, the limitation of this method can be explained that the tensile strength theory is only used as the failure criterion of roof in this manuscript. However, He (2009) proved that the critical thickness of tensile failure roof is much greater than that of the punching failure roof when the safe thickness of the thick roof need to be calculated. It means that this limitation can be ignored in this calculation. In terms of Jiangcang No. 1 Coal Mine, it is reasonable to adopt thick plate to analyze the mechanism of permafrost roof broken. Fig. 7 exhibits the thick plate mechanical model of overlying permafrost.

It should be noted that *h* and *q* are the width of the overlying permafrost and overlying uniform distributed loading, respectively. With the mining of coal seam, the midpoints of the long sides (0, ±*w*/2) and short sides (0, ±*l*/2) of the overlying permafrost roof successively transformed into plastic state and its range expanded along their respective boundaries to form the plastic hinge. Finally, all the four boundaries turn into freely rotating hinge boundaries, and the boundary condition was changed from fixed state to simply supported state as shown in Fig. 8. *l* and *w* are the length and width of the overlying permafrost, respectively. However, the boundary constraints preferred to weaken rather than failure for overall permafrost roof.

According to Vlazov thick plate theory, the equilibrium differential equation of simply supported rectangular thick plate can be shown as follows

$$\begin{cases} \dfrac{D}{5}\left[(1-\mu)\nabla^2\psi_x+(1+\mu)\dfrac{\partial\Phi}{\partial x}+\dfrac{1}{2}\dfrac{\partial}{\partial x}\left(\nabla^2\omega\right)\right]+\dfrac{Gh}{3}\left(\dfrac{\partial\omega}{\partial x}-\psi_x\right)=0 \\ \dfrac{D}{5}\left[(1-\mu)\nabla^2\psi_y+(1+\mu)\dfrac{\partial\Phi}{\partial y}+\dfrac{1}{2}\dfrac{\partial}{\partial y}\left(\nabla^2\omega\right)\right]+\dfrac{Gh}{3}\left(\dfrac{\partial\omega}{\partial y}-\psi_y\right)=0 \end{cases} \tag{10}$$

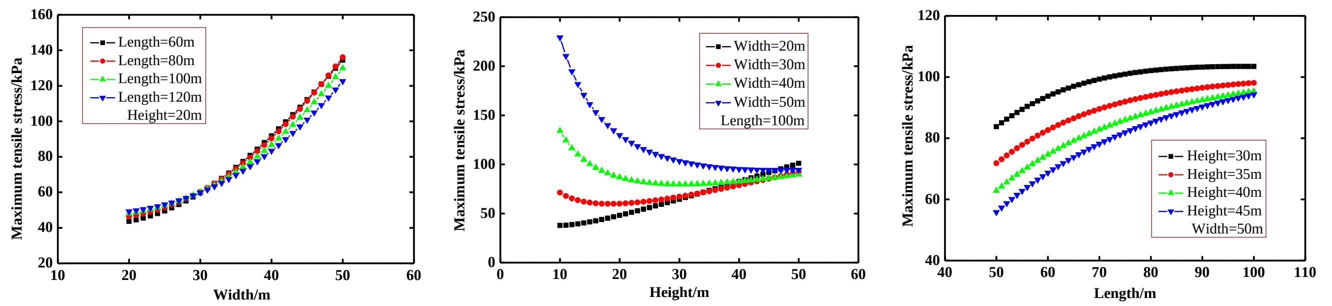

(a) Maximum tensile stress versus width (b) Maximum tensile stress versus height (c) Maximum tensile stress versus length

Fig. 9 Maximum tensile stress versus physical parameters

where ω is the deflection of the thick plate. Ψ_x and Ψ_y are the angles of the straight line on the roof in the XZ and YZ plane. At the same time, $\Phi=\frac{\partial\psi_x}{\partial x}+\frac{\partial\psi_y}{\partial y}$. D is the bending stiffness of the thick plate presented as Eq. (11).

$$D = Eh^3/12(1-\mu^2) \tag{11}$$

$$\sigma_{t\max}=\frac{3q\left(5w^2+4\mu lw+\mu l^2\right)}{10\pi^2\left(\frac{l}{w}+\frac{w}{l}\right)^2 h^2}+\frac{6q\mu\left(l^2-lw\right)}{25(1-\mu)\left(l^2+w^2\right)} \tag{12}$$

Some scholars had taken the derivation of the thick plate problem under similar circumstances (He 2009; Zhao and Zhou 2015). The result showed that the maximum tensile stress occurred on the lower surface and the maximum tensile stress could be represented as Equation (12).

Due to the frozen soil on the surface, there is no extra loading but only considering its own weight. Therefore, the overlying uniform distributed loading can be demonstrated as follows

$$q=\rho gh \tag{13}$$

Substituting Eq. (13) into Eq. (12) can obtain the final expression of maximum tensile stress as follows

$$\sigma_{t\max}=\frac{3\rho g\left(5w^2+4\mu lw+\mu l^2\right)}{10\pi^2\left(\frac{l}{w}+\frac{w}{l}\right)^2 h}+\frac{6\mu\rho gh\left(l^2-lw\right)}{25(1-\mu)\left(l^2+w^2\right)} \tag{14}$$

4.2 Theoretical model analysis

According to the above described, it can be found that the maximum tensile stress of overlying permafrost mainly determines on the parameters of length (l), width (w), density (ρ), thickness (h) and Poisson's ratio (μ) of plate. Among these parameters, the values of density and Poisson's ratio depends on the intrinsic properties of material keeping constant varying with temperature and moisture content. Therefore, the variable-controlling method is used to analyze the influence of other three factors on the maximum tensile stress. Fig. 9 shows the curve of the maximum tensile stress versus each variable.

As shown in Fig. 9(a), the maximum tensile stress increases with the increase of the width of overlying permafrost roof along with the growth rate also increasing. It can be explained that its own gravity and width span of permafrost layer increase inevitably leading to the rise of maximum tensile stress at the lower surface of the overlying permafrost roof. In this case, the roof is easier to break and collapse. Moreover, there is critical width value for giving rise to the maximum tensile stress increasing with the increase of length when the width of overlying permafrost is less than this critical value as well as opposite results occur when the width of overlying permafrost is larger than this critical value.

In terms of Fig. 9(b), the maximum tensile stress decreasing firstly followed by increasing with the increase of height value can be demonstrated. Obviously, the deformation resistance of the thick plate increases with the increase of thickness as a result the maximum tensile stress reduces. On the other hand, the increasing of thickness can cause the self-loading of thick plate increasing and further give rise to the increase of the maximum tensile stress.

Therefore, both of sides together lead to the currently influence results of the height of permafrost layer on the maximum tensile stress. The deformation resistance is of great importance compared with the increase of self-loading leading to the decrease of the maximum tensile stress if the thick plate is thinner. However, the increase of self-loading has a decisive effect when the thick plate increases to a certain value as a result the maximum tensile stress increases with the increase of height continuously.

Fig. 9(c) illustrated the maximum tensile stress versus the length of permafrost roof. It can be found the maximums tensile stress increases with the increase of length value and the increment rate reduces with tending to zero. Similarly, the self-loading and length span of permafrost layer increase with the length of permafrost layer increasing inevitably leading to the increase of the maximum tensile stress at the lower surface of overlying permafrost roof as well as the roof is easier to break.

In terms of Jiangcang No. 1 Coal Mine, the parameters of the overlying permafrost roof after mining are as follows

$$\begin{cases} l=100m \\ w=25m \\ h=30m \end{cases} \tag{15}$$

Considering that after the coal seam was mined, the steeply inclined immediate roof and floor in stope with lower strength may be partially collapsed resulting in an increase in width of overlying permafrost roof. Therefore, the width of the plate should be calculated according to the full collapse of immediate roof and floor considering the safety factor as follows

$$w' = w + w_r + w_f \tag{16}$$

where w' is the maximum width of the overlying permafrost roof, and w, w_r and w_f are the horizontal width of coal seam, immediate roof and immediate floor, respectively. And the values of w_r and w_f are 25.7 m and 1.7 m, respectively. Therefore, the actual parameters of the overlying permafrost roof are as follow.

$$\begin{cases} l = 100m \\ w = 52.4m \\ h = 30m \end{cases} \tag{17}$$

Substituting the above relative parameters into Eq. (14) obtaining the maximum tensile stress of the overlying permafrost roof is 110.83 KPa, which can be compared with the maximum tensile strength of the frozen soil under different temperatures and moisture contents as shown in Table 2. However, the moisture content of the permafrost in Jiangcang No. 1 Coal Mine is over 20%. Meanwhile, the tensile strength of frozen soil increases with the decrease of temperature and the increase of moisture content. Therefore, the minimum tensile strength of the overlying permafrost failure is 190.50 KPa larger than the maximum tensile stress of the overlying permafrost roof in the process of mining when the moisture content is in the range from 20% to 27% and the temperature changes within the range of -35°C~-15°C. That is to say the overlying permafrost roof cannot collapse under this mining conditions.

The number of mining levels studied in this paper is small, and the hard main roof over the immediate roof will not break. However, when the mining depth becomes large, the exposed area of the main roof will increase, which will also lead to the breakage of the main roof. In this case, the overlying permafrost roof may break due to the increase of the exposed area. The parameters of the overlying permafrost roof when the first main roof breaks are as follows

$$\begin{cases} l = 100m \\ w = 80.1m \\ h = 30m \end{cases} \tag{18}$$

Substituting the above relative parameters into equation (14) obtaining the maximum tensile stress of the overlying permafrost roof is 230.46KPa, which is large than the failure tensile strength of it. Therefore, under this condition, the overlying permafrost roof breaks.

Moreover, considering the higher temperature in summer and the potential sudden change of temperature in winter, it is necessary to analyze the stability and safety of overlying permafrost roof under high temperature. Combining with Eq. (1) and (9), the variation trends of maximum tensile stress in thick plate mechanical model and

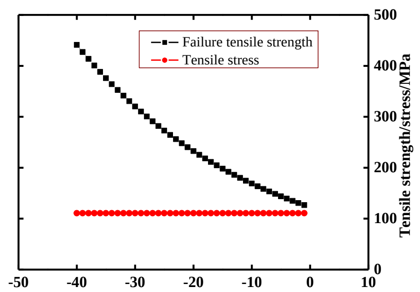

Fig. 10 Failure tensile strength and tensile stress versus temperature

failure tensile strength in overlying permafrost layer with temperature can be illustrated as shown in Fig. 10. Obviously, the failure tensile strength of frozen soil decreases with the increase of temperature, however, which is always greater than the maximum tensile stress calculated by thick plate mechanical model below -1.5°C. And this temperature can be regards as critical point of warm frozen soil. Therefore, the overlying permafrost roof possesses high stability and safety without collapsing in this mining area.

5. Numerical simulation

Surface subsidence due to coal mining is a very complex process depending on the change of time and space. Moreover, different geological conditions and mining conditions also show different characteristics of surface movement and deformation (Antonova *et al*. 2018, Wu *et al*. 2018, Fu *et al*. 2018, Zhou *et al*. 2018b, Wang *et al*. 2018, Yang *et al*. 2019). Therefore, it is very difficult to solve the analytical solution of the surface subsidence by using classical mechanics. In this paper, $FLAC^{3D}$ numerical simulation software was used to calculate and analyze the subsidence of overlying permafrost in Jiangcang No.1 Coal Mine under different conditions.

5.1 Numerical model establishment

Combined with the engineering conditions of Jiangcang No. 1 Coal Mine, the numerical model is established as shown in Fig. 11. To be specific, the thickness of overlying permafrost layer is 30 m. Moreover, the horizontal thickness, dip angle and length along strike of the coal seam are 25m, 55° and 100 m, respectively. According to the actual mining situation, the coal seam is divided into 3 levels for downward mining, and the length of each subsection is 16 m, 17 m and 17 m, respectively, as shown in Fig. 11(b). Meanwhile, the mining area is relative small with size of 180 m ×160 m. Therefore, its ice content in horizontal direction can be neglected. With the increase of moisture content, the tensile strength of frozen soil increases as well. Therefore, the minimum moisture content 20% can be selected for evaluating the stability and safety of permafrost layer. And it is not necessary to consider the change of moisture content in vertical direction. Considering the boundary effect, the model sizes in the directions of length, width and height are determined to take

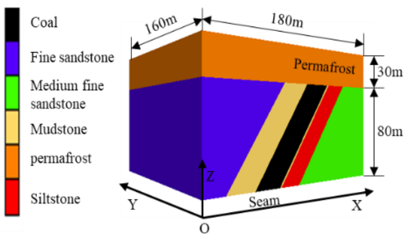

(a) Numerical model

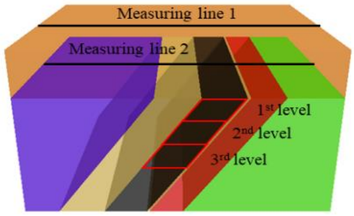

(b) Measuring line layout

Fig. 11 Details of numerical model

Table 4 Mechanical parameters of rock strata in numerical model

Rock type	Volume weight (kN/m^3)	Elastic Modulus /GPa	Tensile strength /MPa	Poisson's ratio	Cohesion /MPa	Friction angle/°
Medium fine sandstone	27.6	27.5	1.50	0.22	3.20	35
Fine sandstone	28.7	33.4	3.78	0.24	3.20	42
Mudstone	24.8	17.7	0.58	0.20	1.20	33
Coal	13.3	5.3	0.15	0.32	1.25	32
Siltstone	24.6	19.5	1.84	0.20	2.75	38

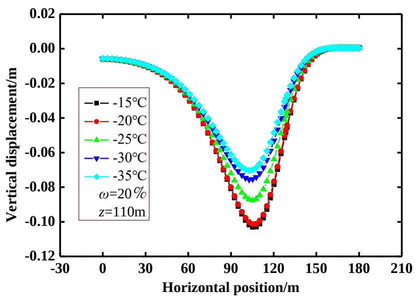

(a) Measuring line 1

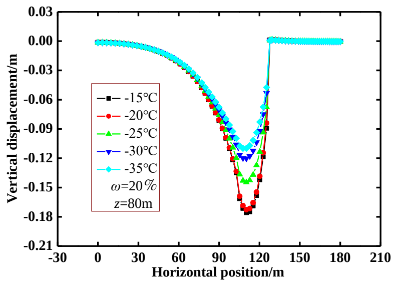

(b) Measuring line 2

Fig. 12 Permafrost subsidence with different temperatures

180 m×160 m×110 m, respectively. The main mechanical parameters of rock strata in the numerical model are shown in Table 4.

The whole model is symmetric about y=80 m plane. Due to the deformation characteristics of the thick plate structure that maximum subsidence occurs on the midline of the long side of the thick plate, the maximum subsidence occurs on the intersection line between the plane and the overlying permafrost. Two measuring lines as shown in Fig. 11(b) are arranged on the upper and lower boundaries of the permafrost layer and its expression are Eq. (18) as follows

$$l_1:\begin{cases} y=80\text{m} \\ z=80\text{m} \end{cases} \qquad l_2:\begin{cases} y=80\text{m} \\ z=110\text{m} \end{cases} \tag{19}$$

5.2 The law of permafrost subsidence under different temperature

According to Table 3, the basic mechanical parameters of permafrost layer with different temperatures in the numerical model are adjusted. Therefore, the numerical results of vertical displacement of permafrost layer with different temperatures can be obtained as shown in Fig. 12.

Keeping the moisture content with 20% and varying the temperature in the range from -35 °C to -15 °C, the maximum subsidence of the upper boundary is -0.1031 m, -0.1013 m, -0.0875 m, -0.0755 m, -0.0703 m, and the maximum subsidence of the lower boundary is -0.1758 m, -0.1728 m, -0.1448 m, -0.1202 m, -0.1090 m at -15 °C, -20 °C, -25 °C, -30 °C, -35 °C, respectively, which indicated the overlying permafrost decreases with the decrease of temperature. As said before, the temperature can affect the elastic modulus which further causes the deformation of overlying permafrost in different degree. However, the maximum subsidence of the upper boundary (z=110 m) of the overlying thick permafrost is smaller than that of the lower boundary (z=80 m). The maximum subsidence in both boundaries occurs above the first level of goaf. To be specific, the maximum subsidence at the upper and lower boundaries of the overlying permafrost are at x=105 m, x=110 m plane, respectively. That is to say the position of maximum subsidence at the upper boundary is on the right side of that of lower boundary. Since the coal seam is a steeply inclined coal seam, the surface subsidence curve is asymmetrically distributed. Overall, the changing trend of vertical displacement on the left side of the maximum subsidence position is slower than that of the right side.

5.3 The law of permafrost subsidence under different temperature

Similarly, the mechanical parameters of permafrost layer with different moisture contents in numerical model are adjusted based on Table 3. Therefore, the surface subsidence varying with moisture content is obtained as shown in Fig. 13.

Figs. 13(a) and 13(b) illustrates the maximum subsidence of the upper boundary is -0.0994 m, -0.0875 m, -0.0817 m, -0.0740 m, -0.0701 m at the moisture content of 15%, 20%, 22%, 25%, 27%, respectively, as well as the maximum subsidence at the lower boundary is -0.1691 m, -0.1450 m, -0.1335 m, -0.1172 m, -0.1097 m at the corresponding moisture content, respectively, with the

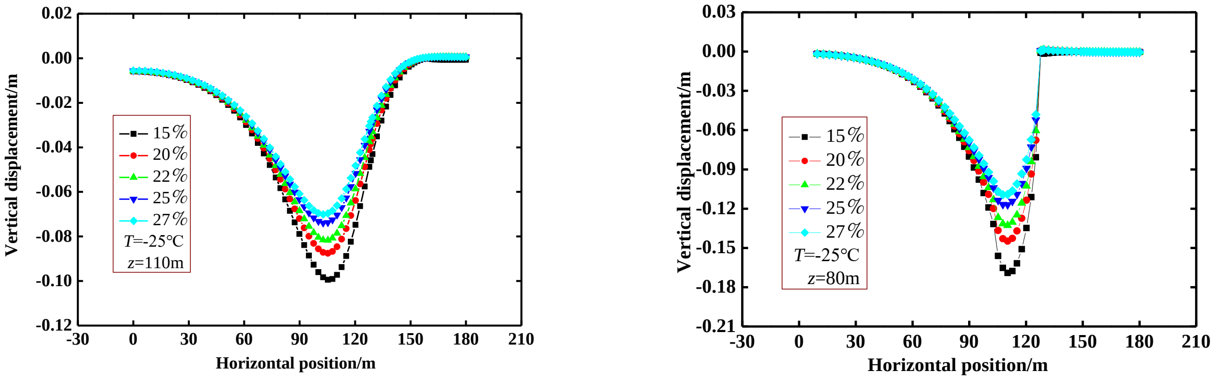

(a) Measuring line 1 (b) Measuring line 2

Fig.13 Permafrost subsidence under different moisture contents

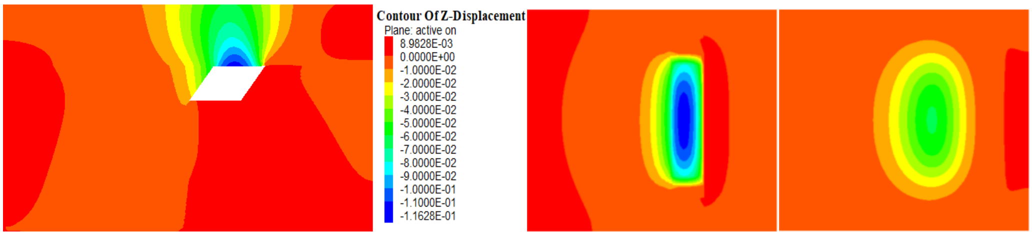

(a) After first subsection mined

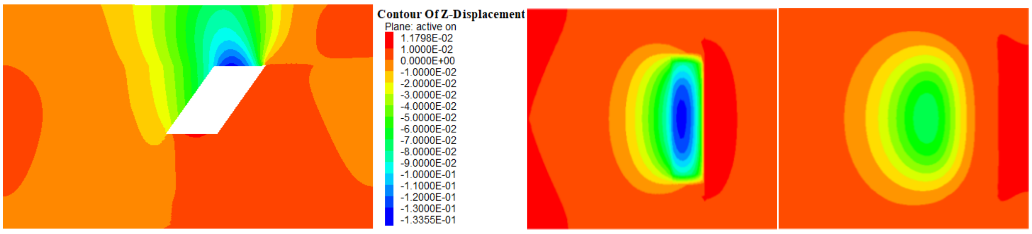

(b) After second subsection mined

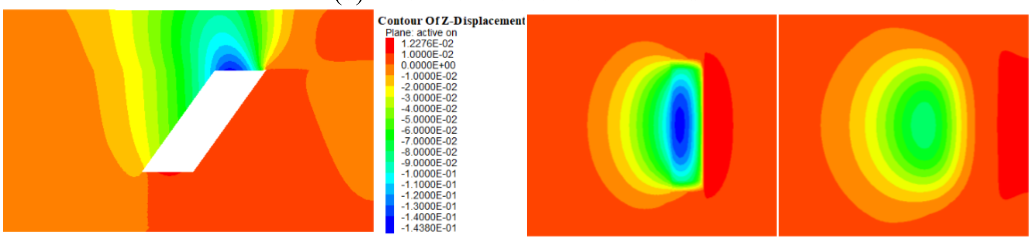

(c) After third subsection mined

Fig.14 Vertical displacement contour of overlying permafrost

temperature keeping -25°C. It demonstrates the maximum subsidence on both of positions decreases with the increase of moisture content as a result of the elastic modulus as vital factor for the deformation of the overlying permafrost increases with the increase of moisture content. However, the maximum subsidence of the upper boundary (z=110 m) is smaller than that of the lower boundary (z=80 m). The maximum subsidence on both of positions occurs above the first level of the goaf. Moreover, the position of maximum subsidence at the upper boundary is on the right side compared with lower boundary because the maximum subsidence at the upper boundary of the overlying permafrost is at x=105 m, while x=110 m can be obtained the maximum subsidence at the lower boundary. Since the coal seam is a steeply inclined coal seam, the surface subsidence curve is asymmetrically distributed. Overall, the changing trend of vertical displacement on the left side of the maximum subsidence position is slower compared with that of right side.

5.4 The subsidence law of subsection mining

5.4.1 Vertical displacement of overlying permafrost

As said above, the dip angle of main coal seam in Jiangcang No. 1 Coal Mine is 55° belonging to steeply inclined coal seam. Therefore, it is divided into 3 horizontal levels for downward mining, and the length of each subsection is 16 m, 17 m and 17 m, respectively. Taking the case of temperature -25°C and moisture content 20% as example, the subsidence law of overlying permafrost after each subsection mined are investigated and analyzed by using numerical simulation. The results of vertical

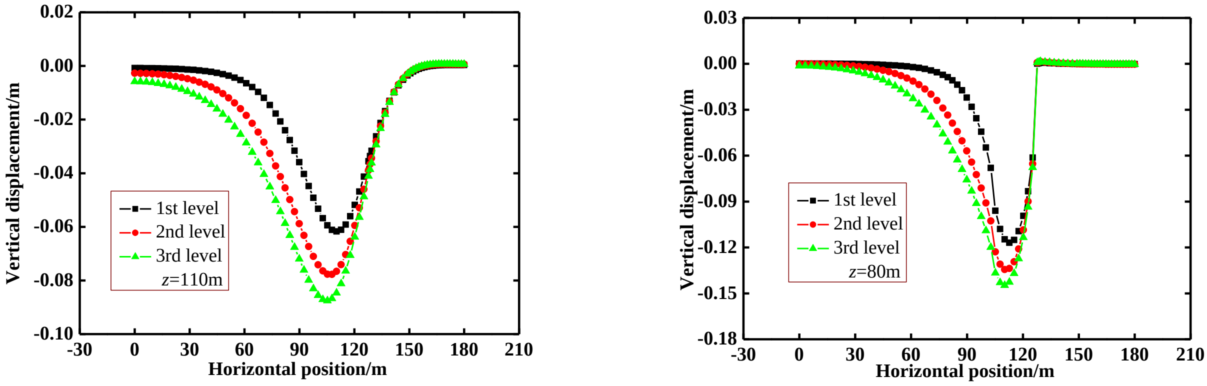

(a) Measuring line 1 (b) Measuring line 2

Fig.15 Permafrost subsidence after each subsection mining

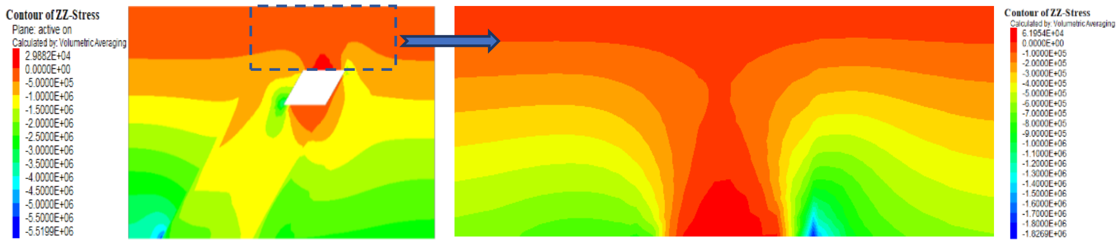

(a) After first subsection mined

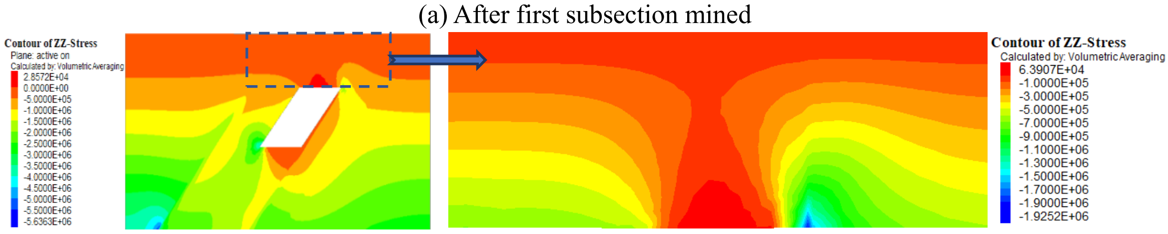

(b) After second subsection mined

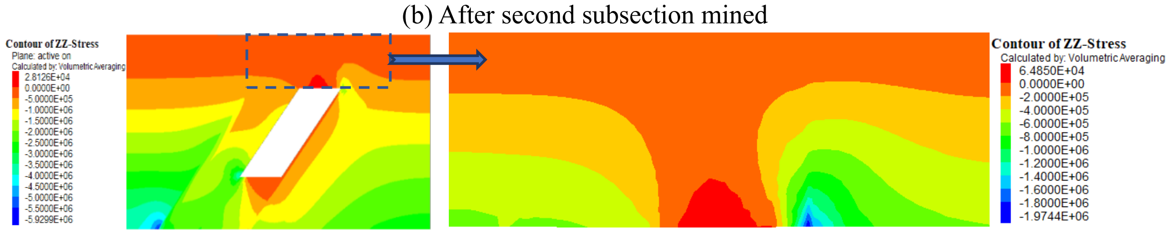

(c) After third subsection mined

Fig.16 Vertical stress contour of overlying permafrost

displacement contour selecting the plane of y=80 m (left), z=80 m (center) and z=110 m (right) after each subsection mined, respectively, are shown in Fig. 14.

The subsidence of overlying permafrost is asymmetrical after the first subsection mined (Fig. 14(a)) as a result of the asymmetric distribution of the strata. Moreover, the values of subsidence of overlying permafrost increase and the position of maximum value moves to the left side after the second subsection mined (Fig. 14(b)) due to the goaf extending to the left with the continuously mining of coal seam. However, the subsidence reaches the maximum value when the third subsection is mined (Fig. 14(c)) and the position of the maximum subsidence continues to move to the left goaf. Further, the maximum subsidence occurs at the lower boundary (z=80 m) of overlying permafrost roof above the goaf compared with upper boundary (z=110 m) through analyzing the vertical displacement curve of permafrost layer after each subsection mined as shown in Fig. 15. It indicated that the left side decreases slowly, while the dramatically reducing can be seen in the right side although the values of subsidence overall decrease on both sides.

5.4.2 Vertical stress of overlying permafrost

The vertical stress contour of overlying permafrost is shown in Fig. 16, which demonstrates the initial stress balance state of overlying strata is destroyed and the stress around stope is redistributed after coal seam mined.

However, it can be seen that the stress of strata and permafrost is asymmetrically distributed due to the coal seam belonging to steeply inclined coal seam. And the upper boundary has marginally change after coal seam mined because of the thick overly permafrost roof existing.

To be specific, there is stress releasing zone where the stress is smaller than the original stress appearing in the lower boundary of permafrost roof above goaf after the first subsection of coal seam mined. Moreover, the stress direction in stress releasing zone is deflected from downward to upward due to shallow depth and larger horizontal stress. At the same time, both sides of near goaf in horizontal direction appearing the phenomenon of stress concentration forms a certain region with elevated stress.

However, the value of peak stress on the left side of goaf is smaller than that of on right side, while its position of peak stress away from goaf on left side is larger than that of on right side in horizontal direction because mudstone and high-strength siltstone occur in the left and right sides of goaf, respectively.

When the second and third subsections of coal mine are mined, the position of peak stress on the right side of permafrost lower boundary has marginal change, while this position on left side further moves to away from goaf due to the goaf extending to the bottom left of working face in the process of coal mining. However, there are minor changing for the value of peak stresses on both sides.

6. Conclusions

Based on the engineering background of Jiangcang No. 1 Coal Mine in permafrost region, this paper presented the influence of temperature and moisture content on the displacement and stress law of frozen soil layer combined with laboratory experiments, theoretical calculation and numerical simulation. The following conclusions can be drawn from the present study.

• Uniaxial compression testing was carried out to obtain the unconfined compressive strength and the elastic modulus of frozen soil under different temperatures and moisture contents. On the other hand, some mechanical parameters, such as bulk modulus, shear modulus, cohesion, internal friction angle and tensile strength can be acquired from field measurements and empirical formula. The results indicated that the unconfined compressive strength and elastic modulus of frozen soil increase with the decrease of temperature and the increase of moisture content based on the currently limited results in laboratory experiments.

• The thick plate mechanical model of overlying permafrost is established to evaluate the safety of the permafrost roof. It demonstrated that the maximum tensile stress occurs on the lower surface. In terms of Jiangcang No. 1 Coal Mine, the maximum tensile stress of the overlying permafrost roof is 110.83 KPa. Compared with the maximum tensile strength of the frozen soil failure under different temperatures and moisture contents, the minimum tensile strength of the overlying permafrost is 190.50KPa, which is obviously larger than the maximum tensile stress of the overlying permafrost roof during the process of mining. Therefore, the overlying permafrost roof cannot collapse under the condition that the moisture content is in the range from 20% to 27% and the temperature changes within the range of -35°C~-15°C.

• Through the results of numerical simulation taking Jiangcang No.1 Coal Mine as engineering background, the maximum subsidence of both upper boundary (z=110m) and lower boundary (z=80 m) decreases with the decrease of temperature and the increase of moisture content with the conditions of moisture content keeping 20% as well as temperature in the range of -35°C~-15°C or the temperature keeping -25°C as well as moisture content in the range from 15% to 27%.

• The main coal seam divided into three subsections. Combined with numerical simulation, it can be found the value of subsidence of overlying permafrost roof increases and the position of maximum subsidence moves to the left side with the successive mining of each subsection continuously. Meanwhile, there is marginally changing for the location of the peak value stress on the right side of the permafrost lower boundary, while the location of the peak value stress tends to away from workface on the left side of the permafrost lower boundary. However, the peak value stresses on both sides have minor change.

Acknowledgements

The authors wish to acknowledge the support from the National Key Research and Development Program of China (No. 2017YFC0603002) and the General Program of National Natural Science Foundation of China (No. 51574244 & No. 51674264) as well as China Scholarship Council. The authors would also like to thank the editors and anonymous reviewers for their valuable time and suggestions.

References

Álvarez-Fernández, M.I., González-Nicieza, C., Menéndez-Díaz, A. and Álvarez-Vigil, A.E. (2005), “Generalization of the n–k influence function to predict mining subsidence”, *Eng. Geol.*, **80**(1-2), 1-36. https://doi.org/10.1016/j.enggeo.2005.02.004.

Ambrožič, T. and Turk, G. (2003), “Prediction of subsidence due to underground mining by artificial neural networks”, *Comput. Geosci.*, **29**(5), 627-637. https://doi.org/10.1016/S0098-3004(03)00044-X.

Andersland, O.B. and Akili, W. (2015), “Stress effect on creep rates of a frozen clay soil”, *Géotechnique*, **17**(1), 27-39. https://doi.org/10.1680/geot.1967.17.1.27.

Antonova, S., Sudhaus, H., Strozzi, T., Zwieback, S., Kääb, A., Heim, B., and Boike, J. (2018), “Thaw subsidence of a yedoma landscape in northern Siberia, measured in situ and estimated from TerraSAR-X interferometry”, *Remote Sens.*, **10**(4), 494. https://doi.org/10.3390/rs10040494.

Azadegan, O., Li, J. and Jafari, S.H. (2014), “Estimation of shear strength parameters of lime-cement stabilized granular soils from unconfined compressive tests”, *Geomech. Eng.*, **7**(3), 247-261. https://doi.org/10.12989/gae.2014.7.3.247

Azmatch, T.F., Sego, D.C., Arenson, L.U. and Biggar, K.W. (2011), “Tensile strength and stress-strain behaviour of Devon silt under frozen fringe conditions”, *Cold Reg. Sci. Technol.*, **68**(1-2), 85-90. https://doi.org/10.1016/j.coldregions.2011.05.002

Azmatch, T.F., Sego, D.C., Arenson, L.U. and Biggar, K.W. (2012), “Using soil freezing characteristic curve to estimate the hydraulic conductivity function of partially frozen soils”, *Cold Reg. Sci. Technol.*, **83-84**, 103-109. https://doi.org/10.1016/j.coldregions.2012.07.002.

Chang, I., Im, J., Prasidhi, A.K. and Cho, G.C. (2015), “Effects of Xanthan gum biopolymer on soil strengthening”, *Constr. Build. Mater.*, **74**, 65-72.

https://doi.org/10.1016/j.conbuildmat.2014.10.026.
Chen, J., Du, C., Jiang, D., Fan, J. and He, Y. (2016), "The mechanical properties of rock salt under cyclic loading-unloading experiments", *Geomech. Eng.*, **10**(3), 325-334. https://doi.org/10.12989/gae.2016.10.3.325.
Cheng, X.S. (1989), *Applied Theory of Plates and Shells*, Shandong Science & Technology Press, Ji'nan, China (in Chinese).
Cheng, Z.B., Zhang, Y.N., Li, L.H. and Lv, H.Y. (2018), "Theoretical solution and analysis of the elastic modulus and foundation coefficient of coal-rock combination material", *Int. J. Mater. Sci Res.,* **1**(1), 23-31.
Christ, M. and Kim, Y. (2009), "Experimental study on the physical-mechanical properties of frozen silt", *KSCE J. Civ. Eng.*, **13**(9), 317-324. https://doi.org/10.1007/s12205-009-0317-z.
Dai, H.D., Yin, M.L., He, T.Y., Liu, k., Li, T. and Zheng, T.Q. (2014), "Research on the mechanical and thermophysical properties of frozen Soil in cretaceous formation", *Appl. Mech. Mater.*, **580-583**, 962-965. https://doi.org/10.4028/www.scientific.net/AMM.580-583.962.
Evans, S.G., Ge, S., Voss, C.I., and Molotch, N.P. (2018), "The role of frozen soil in groundwater discharge predictions for warming alpine watersheds", *Water Resour. Res.*, **54**(3), 1599-1615. https://doi.org/10.1002/2017WR022098.
Fu, Q., Wang, E., Li, T., and Hou, R. (2018), "Impact factors and dynamic simulation of tillage-layer temperature in frozen-thawed soil under different cover conditions", *Int. J. Agr. Biol. Eng.*, **11**(2), 101-107.
Hatheway, H.W. (2009), "The complete ISRM suggested methods for rock characterization, testing and monitoring, 1974-2006", *Environ. Eng. Geosci.*, **15**(1), 47-48. https://doi.org/10.2113/gseegeosci.15.1.47.
He, G.L. (2009), "Determination of critical thickness of stiff roof in coal mine based on thick plate theory", *Chin. J. Undergr. Sp. Eng.*, **5**(4), 659-664 (in Chinese).
Hejmanowski, R. and Malinowska, A. (2009), "Evaluation of reliability of subsidence prediction based on spatial statistical analysis", *Int. J. Rock Mech. Min.*, **46**(2), 432-438. https://doi.org/10.1016/j.ijrmms.2008.07.012.
Li, G.D., Zhang, H.S. and Li, H.H. (2013), "The comparative analysis of probability integration and numerical simulation in surface subsidence prediction", *Appl. Mech. Mater.*, **295-298**, 3015-3018. https://doi.org/10.4028/www.scientific.net/AMM.295-298.3015.
Li, H., Zhu, Y., Zhang, J. and Lin, C. (2004), "Effects of temperature, strain rate and dry density on compressive strength of saturated frozen clay", *Cold Reg. Sci. Technol.*, **39**(1), 39-45.
Li, P.X., Tan, Z.X., Yan, L.L. and Deng, K.Z. (2011), "Time series prediction of mining subsidence based on a SVM", *Int. J. Rock Mech. Min. Sci*., **21**(4), 557-562. https://doi.org/10.1016/j.mstc.2011.02.025.
Liu, F., Guo, Z.R., Lv, H.Y., and Cheng, Z.B. (2018), "Test and analysis of blast wave in mortar test block", *Int. J. Rock Mech. Min. Sci.*, **108**, 80-85. https://doi.org/10.1016/j.ijrmms.2018.06.003.
Liu, X.J. and Cheng, Z.B. (2019), "Changes in subsidence-field surface movement in shallow-seam coal mining", *J. S. Afr. I. Min. Metall.*, **119**(2), 201-206. http://dx.doi.org/10.17159/2411-9717/2019/v119n2a12.
Lv, H.Y., Tang, Y.S., Zhang, L.F., Cheng, Z.B. and Zhang, Y.N. (2019), "Analysis for mechanical characteristics and failure models of coal specimens with non-penetrating single crack", *Geomech. Eng.*, **17**(4), 355-365. https://doi.org/10.12989/gae.2019.17.4.355.
Nie, L., Wang, H., Xu, Y. and Li, Z. (2015), "A new prediction model for mining subsidence deformation: the arc tangent function model", *Nat. Hazards*, **75**(3), 2185-2198. https://doi.org/10.1007/s11069-014-1421-z.
Qin, S., Wang, S., Long, H., Liu, J., Qin, S. and Wang, S. (1999), "A new approach to estimating geo-stresses from laboratory Kaiser effect measurements", *Int. J. Rock Mech. Min.*, **36**(8), 1073-1077. https://doi.org/10.1016/S1365-1609(99)00068-4.
Shang, T.L., Suo, Y.L. and Liu, Y.W. (2017), "Research on ascending mining in multiple coal seams under permafrost", *Coal Technol.*, **36**(7), 20-22 (in Chinese).
Suo, Y.L. and Fan, Q.Q. (2014), "Study on rational exploiting elevation limit of coal mine with permafrost layer", *Coal Technol.*, **33**(5), 149-151 (in Chinese).
Sun, W.B., Du, H.Q., Zhou, F., and Shao, J.L., (2019), "Experimental study of crack propagation of rock-like specimens containing conjugate fractures", *Geomech. Eng.*, **17**(4), 323-331. https://doi.org/10.12989/gae.2019.17.4.323.
Tu, Y.L., Zhong, Z.L., Luo, W.K., Liu, X.R. and Wang, S. (2016), "A modified shear strength reduction finite element method for soil slope under wetting-drying cycles", *Geomech. Eng.*, **11**(6), 739-756. https://doi.org/10.12989/gae.2016.11.6.739.
Viso, J.R.D., Carmona, J.R. and Ruiz, G. (2008), "Shape and size effects on the compressive strength of high-strength concrete", *Cement Concrete Res.*, **38**(3), 386-395. https://doi.org/10.1016/j.cemconres.2007.09.020Get.
Wang, M., Meng, S., Yuan, X., Sun, Y., and Zhou, J. (2018), "Experimental validation of vibration-excited subsidence model of seasonally frozen soil under cyclic loads", *Cold Reg. Sci. Technol.*, **146**, 175-181. https://doi.org/10.1016/j.coldregions.2017.11.001.
Wang, T., Zhou, G., Wang, J. and Yin, L. (2017), "Stochastic thermal-mechanical characteristics of frozen soil foundation for a transmission line tower in permafrost regions", *Int. J. Geomech.*, **18**(3), 06017025. https://doi.org/10.1061/(ASCE)GM.1943-5622.0001087.
Wang, Z.H. and Cheng, Z.B. (2016), "Hard roof fracturing form and dynamic disaster control in short island mining face", *Chin. J. Rock Mech. Eng.*, **35**(S2), 4018-4028 (in Chinese).
Wu, X., Zhao, L., Liu, G., Xu, H., Zhang, X. and Ding, Y. (2018), "Effects of permafrost thaw-subsidence on soil bacterial communities in the southern Qinghai-Tibetan Plateau", *Appl. Soil Ecol.*, **128**, 81-88. https://doi.org/10.1016/j.apsoil.2018.04.007.
Xu, H., Liu, B. and Fang, Z. (2014), "New grey prediction model and its application in forecasting land subsidence in coal mine", *Nat. Hazards*, **71**(2), 1181-1194. https://doi.org/10.1007/s11069-013-0656-4.
Xu, N., Kulatilake, P.H.S.W., Tian, H., Wu, X., Nan, Y. and Wei, T. (2013), "Surface subsidence prediction for the WUTONG mine using a 3-D finite difference method", *Comput. Geotech.*, **48**(3), 134-145. https://doi.org/10.1016/j.compgeo.2012.09.014.
Xu, G., Wu, W., Kong, L. and Qi, J. (2018), "Hypoplastic modeling for the mechanical behavior of frozen soil in stress path testing", *Int. J. Geomech.*, **18**(6), 04018049. https://doi.org/10.1061/(ASCE)GM.1943-5622.0001117.
Yang, S.L., Wang, Z.H., Kong, D.Z., Cheng, Z.B. and Song, G.F., (2016), "Overlying strata failure process and support resistance determination in large mining height face", *Chin. J. Rock Mech. Eng.*, **33**(2), 199-207. (in Chinese)
Yang, X., Wen, G., Dai, L., Sun, H. and Li, X. (2019), "Ground subsidence and surface cracks evolution from shallow-buried close-distance multi-seam mining: a case study in Bulianta Coal Mine", *Rock Mech. Rock Eng.,* 1-18. https://doi.org/10.1007/s00603-018-1726-4.
Yao, Y., Chen, J., Li, T., Fu, B., Wang, H., Li, Y. and Jia, H. (2019), "Soil liquefaction in seasonally frozen ground during the 2016 Mw6.6 Akto earthquake", *Soil Dyn. Earthq. Eng.*, **117**, 138-148. https://doi.org/10.1016/j.soildyn.2018.08.024.

Yoshimoto, N., Wu, Y., Hyodo, M. and Nakata, Y. (2016), "Effect of relative density on the shear behavior of granulated coal ash", *Geomech. Eng.*, **10**(2), 207-224. https://doi.org/10.12989/gae.2016.10.2.207.

Zhao, G. and Zhou, S. (2015), "Determining safe thickness of roof in subsea mining based on thick plate theory", *Chin. J. Geological Hazard Control*, **26**(4), 60-66.

Zhou, D., Wu, K., Miao, X. and Li, L. (2018a), "Combined prediction model for mining subsidence in coal mining areas covered with thick alluvial soil layer", *B Eng. Geol. Environ.*, **77**(1), 283-304. https://doi.org/10.1007/s10064-016-0961-8.

Zhou, Z., Yang, H., Xing, K., and Gao, W. (2018b), "Prediction models of the shear modulus of normal or frozen soil-rock mixtures", *Geomech. Eng.*, **15**(2), 783-791. https://doi.org/10.12989/gae.2018.15.2.783.

CC